CHEMISTRY
A EUROPEAN JOURNAL

DOI: 10.1002/chem.200701357

A Versatile Ditopic Ligand System for Sensitizing the Luminescence of Bimetallic Lanthanide Bio-Imaging Probes

Anne-Sophie Chauvin,* Steve Comby, Bo Song, Caroline D. B. Vandevyver,* and Jean-Claude G. Bünzli*[a]

Abstract: The homoditopic ligand 6,6′-[methylenebis(1-methyl-1*H*-benzimidazole-5,2-diyl)]bis(4-{2-[2-(2-methoxyethoxy)ethoxy]ethoxy}pyridine-2-carboxylic acid) (H_2L^{C2}) has been tailored to self-assemble with lanthanide ions (Ln^{III}), which results in the formation of neutral bimetallic helicates with the overall composition $[Ln_2(L^{C2})_3]$ and also provides a versatile platform for further derivatization. The grafting of poly(oxyethylene) groups onto the pyridine units ensures water solubility, while maintaining sizeable thermodynamic stability and adequate antenna effects for the excitation of both visible- and NIR-emitting Ln^{III} ions. The conditional stability constants ($\log\beta_{23}$) are close to 25 at physiological pH and under stoichiometric conditions. The ligand triplet state features adequate energy (0-phonon transition at $\approx 21\,900\ cm^{-1}$) to sensitize the luminescence of Eu^{III} ($Q = 21\,\%$) and Tb^{III} (11 %) in aerated water at pH 7.4. The emission of several other VIS- and NIR-emitting ions, such as Sm^{III} ($Q = 0.38\,\%$) or Yb^{III} (0.15 %), for which in cellulo luminescence is evidenced for the first time, is also sensitized. The Eu^{III} emission spectrum arises from a main species with pseudo-D_3 symmetry and without coordinated water. The cell viability of several cancerous cell lines (MCF-7, HeLa, Jurkat and 5D10) is unaffected if incubated with up to 500 μM $[Eu_2(L^{C2})_3]$ during 24 h. Bright Eu^{III} emission is seen for incubation concentrations above 10 μM and after a 15-minute loading time; similar images are obtained with Tb^{III} and Sm^{III}. The helicates probably permeate into the cytoplasm of HeLa cells by endocytosis. The described luminescent helical stains are robust chemical species which remain undissociated in the cell medium and in presence of other complexing agents, such as edta, dtpa, citrate or L-ascorbate. Their derivatization, which would open the way to the sensing of targeted in cellulo phenomena, is currently under investigation.

Keywords: helical structures · heterometallic complexes · imaging agents · lanthanides · luminescence

Introduction

Some of the most important aspects of biochemistry, bioengineering, drug design, and medical diagnosis include the study and sensing of in cellulo phenomena,[1] the mapping of selected or targeted analytes,[2,3] the elucidation of receptor–ligand interactions,[4] and the imaging of organs and cells.[5,6] Luminescence-based analytical methods are among the most sensitive for these purposes and the distinctive properties of trivalent lanthanide ions,[7] especially their ability to lend themselves to time-resolved detection in order to eliminate all background signals and autofluorescence, are of particular interest. This behavior is well established for luminescence immunoassays[8–11] and has been described in numerous reviews during the last decade.[7–13] Extension to the use of near-infrared (NIR)-emitting lanthanide bioprobes has added another exciting dimension to this field.[12–14]

Several strategies have been developed to encapsulate trivalent lanthanide ions into functional molecular structures in order to meet the stringent requirements imposed on luminescent bioprobes, namely high thermodynamic stability and kinetic inertness under physiological conditions, coupling and targeting ability, as well as the tuning and/or switching of key photophysical properties, in addition to non-toxicity, cell permeability and resistance to photobleaching.[15] The corresponding host molecules may be divided into five categories (polyaminocarboxylates,[10] bipyri-

[a] Dr. A.-S. Chauvin, S. Comby, Dr. B. Song, Dr. C. D. B. Vandevyver, Prof. Dr. J.-C. G. Bünzli
Laboratory of Lanthanide Supramolecular Chemistry
école Polytechnique Fédérale de Lausanne (EPFL)
LCSL-BCH 1401 (Switzerland)
Fax: (+41) 21-693-9825
E-mail: anne-sophie.chauvin@epfl.ch
caroline.vandevyver@epfl.ch
jean-claude.bunzli@epfl.ch

Supporting Information for this article is available on the WWW under http://www.chemeurj.org/ or from the author.

dine-based cryptands,[16] cyclen derivatives containing coordinating and sensitizing groups,[17] aza-macrocycles incorporating a pyridine, bipyridine or terpyridine unit[18,19] and β-diketonates[20]), which often have in common the simultaneous use of carboxylate (or amide) and amine coordinating groups.

Initial experiments on cell imaging with lanthanide chelates have involved the staining of bacterial smears from *E. Coli* cell walls,[21] time-resolved studies of 3T3 cultured cells,[22] and the detection of malignant tumors in C-57 dark-fur mice with the help of Yb^{III} NIR emission.[23] Eu^{III} probes have helped to elucidate the nature of the binding sites on the cell walls of *Datura innoxia*[24] and to map the receptor-activated heat waves in Chinese hamster ovaries by a thermal imaging technique.[25] Tb^{III}-based chelates have also proved useful, as exemplified by a lipid-conjugated chelate that functions as a membrane-staining agent in morphological studies of Swiss albino mouse 3T3 cultured cells,[22] or by Bornhop's high brightness macrocyclic labels for in vitro and in vivo analysis of abnormal tissues.[18,26,27] More recently, Parker and co-workers have designed Eu^{III} complexes that specifically stain the nucleoli of several cell lines (CHO, COS, NIH 3T3, HeLa, and HDF).[15,28–30]

Most lanthanide ions are also paramagnetic and possess an anisotropic susceptibility tensor that makes them useful for the structural investigation of axial complexes[31] or proteins[32] by NMR spectroscopy, while Gd^{III} has emerged as a universal contrast agent for 3D imaging of biological structures (MRI).[33,34] Combining luminescent and magnetic properties in a single probe system is therefore, an attractive way of integrating the advantages of both molecular imaging techniques. This can be done by attaching an organic luminophore onto a contrast agent[35,36] or by developing receptors that are able to bind Gd^{III} and luminescent Ln^{III} ions while preserving the specific physical properties of the metal ions.[19,37,38] Some of these systems bear a targeting vector for cell internalization.[39] Alternatively, the attachment of two magnetic or two luminescent lanthanide ions onto a biologically relevant molecule, such as a protein, brings definitive advantages, as demonstrated recently by the generation of peptide-linked double lanthanide binding tags, which proved to be superior to single tags with respect to luminescence output[40] and X-ray scattering power.[41]

We are engaged in a strategy aimed at incorporating two lanthanide ions into a single molecular triple-stranded helical structure by thermodynamically controlled self-assembly processes.[42] The resulting homo- or heterobimetallic structures are amenable to functionalization for covalent biological coupling and/or targeting purposes. The spectroscopic properties of the Ln^{III} ions inserted into these helicates[43] are fully retained thanks to the protective wrapping of the ligand strands around the metal ions. We have built a library of hexadentate ditopic ligands with bis(benzimidazole)pyridine cores, which induce nine-coordinate, tricapped trigonal-prismatic environments around the 4f ions similar to those found in aqua ions. Some of these molecules are unsymmetrical and are tailored for the recognition of a heteropair of lanthanide ions[44–46] with the aim of developing heterometallic bimodal probes, although this approach is currently limited to organic solvents. A second series of receptors are symmetrical and are based on the parent ligand H_2L^C (Scheme 1), which yields very stable neutral homobimetallic

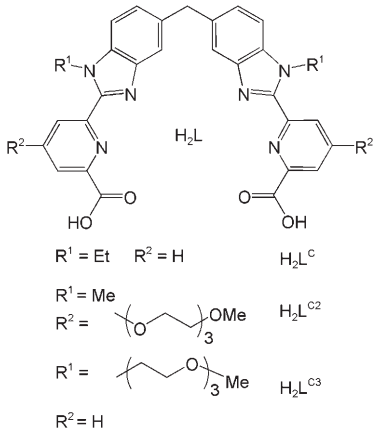

Scheme 1. Structures of the homoditopic hexadentate ligands.

$[Ln_2(L^C)_3]$ helicates in water, with the Eu^{III} complex having particularly interesting photophysical properties (quantum yield = 24 %, $Eu(^5D_0)$ lifetime = 2.43 ms;[47] note that the initially published quantum yield is incorrect and has been redetermined by an absolute method; see Experimental Section).

The new chemistry we are now developing allows multipurpose derivatization of this initial ligand and the introduction of solubilizing, chromophoric or coupling groups. We have recently reported that the Eu^{III} helicate formed by the benzimidazole-substituted hexadentate ligand H_2L^{C3} (Scheme 1) is internalized into HeLa cells by endocytosis and stains their cytoplasm.[48] However, better results are obtained by substituting the 4-position of the pyridine units with poly(oxyethylene) groups (H_2L^{C2}),[49] which ensure water solubility and help to avoid potential stacking of the luminescent tags.[10] In addition, H_2L^{C2} is easily amenable to further derivatization for covalent coupling. We present here a versatile synthetic procedure that leads to the isolation of the ditopic receptor as well as thermodynamic, photophysical and stability studies of the resulting bimetallic helicates. The non-cytotoxicity of the $[Eu_2(L^{C2})_3]$ helicate towards four cancerous cell lines is established, and the usefulness of the bimetallic tags (Ln = Sm, Eu, Tb, Yb) for luminescence microscopy of living cells is demonstrated.

Results

Ligand design and characterization: H_2L^{C2} was synthesized according to Scheme 2. The key step in this reaction is the introduction of poly(oxyethylene) substituents in the *para* positions of the pyridine rings. Thus, chelidamic acid (**1**) was

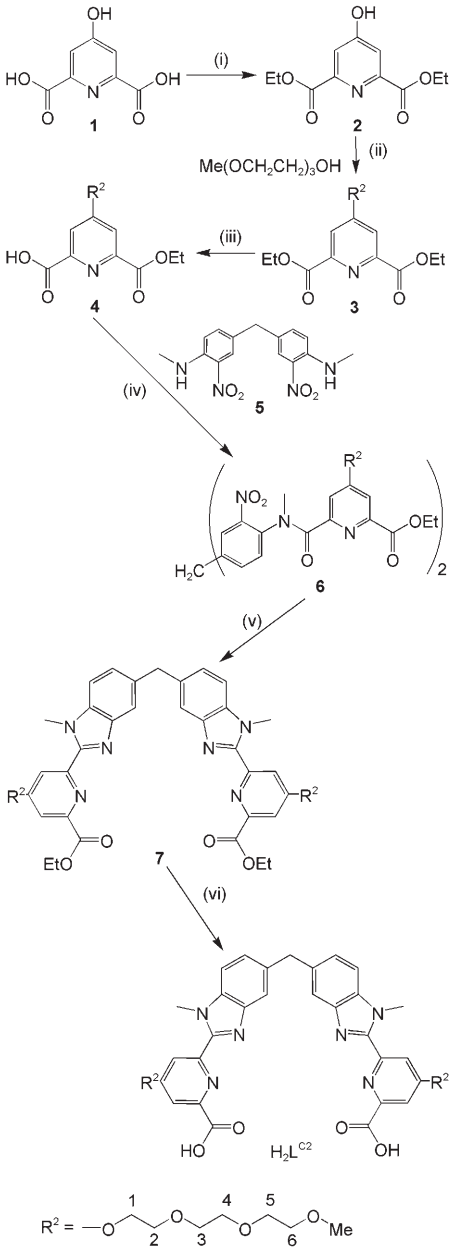

Scheme 2. Synthesis of H_2L^{C2}. Shown at the bottom is the numbering of the methylene groups in the poly(oxyethylene) substituent. (i) H_2SO_4, EtOH, 4 h reflux; (ii) DIAD, PPh_3, thf, 12 h reflux; (iii) NaOH, EtOH, H_2O; (iv) SO_2Cl_2, CH_2Cl_2, dmf, then **5**; (v) Fe, EtOH/H_2O, HCl, then EtOH, H_2SO_4; (vi) NaOH, EtOH.

converted into its diester **2**, and a subsequent Mitsunobu reaction led to the expected functionalization product in reasonable yield (71%). Selective hydrolysis of **3** in the presence of a sub-stoichiometric amount of aqueous NaOH with respect to the carboxylic acid function gave **4**, which was converted into the acyl chloride and then condensed with bis(*N*-methyl nitroaniline) (**5**) in a modified Philips coupling reaction.[50] The resulting disubstituted product **6** was reduced in the presence of iron to give the benzimidazole units of **7**. The difficulties experienced during this step were the removal of the product from the ferric aqueous phase and preventing premature hydrolysis of the diester functions, which leads to an inseparable water-soluble product. Final hydrolysis of the diester functions was performed in a separate step.

The ligand deprotonation constants were determined by spectrophotometric titration of H_2L^{C2} (2.25×10^{-5} M) with sodium hydroxide at constant ionic strength (0.1 M KCl) in the pH range 0.85–12.77 (see Figure S1 in the Supporting Information). The data were successfully fitted to the following set of equations [Eqs. (1–5)], which gave four of the six pK_a values and the sum of the first two:

$$(H_6L^{C2})^{4+} \rightleftharpoons (H_4L^{C2})^{2+} + 2H^+ \qquad (pK_{a1}+pK_{a2})=4.6(1) \qquad (1)$$

$$(H_4L^{C2})^{2+} \rightleftharpoons (H_3L^{C2})^{+} + H^+ \qquad pK_{a3}=3.2(1) \qquad (2)$$

$$(H_3L^{C2})^{+} \rightleftharpoons (H_2L^{C2}) + H^+ \qquad pK_{a4}=4.8(1) \qquad (3)$$

$$(H_2L^{C2}) \rightleftharpoons (HL^{C2})^{-} + H^+ \qquad pK_{a5}=7.7(1) \qquad (4)$$

$$(HL^{C2})^{-} \rightleftharpoons (L^{C2})^{2-} + H^+ \qquad pK_{a6}=11.27(1) \qquad (5)$$

The corresponding distribution diagram is shown in Figure S2 in the Supporting Information. The assignments were made by comparison with H_2L^C, for which only three deprotonation constants [$pK_{a3}=5.4$ (calculated from pK_{a4} by assuming a statistical difference) $pK_{a4}=6.0$, $pK_{a5}=9.5$ and $pK_{a6}=10.1$] could be determined by means of several different experimental techniques, including NMR spectroscopy, owing to solubility problems below pH 6.[51] The largest pK_a values of H_2L^{C2} correspond to deprotonation of the imidazoyl groups and the two middle pK_a values to deprotonation of the pyridyl units, and the more acidic values refer to the carboxylic acid units. A more detailed analysis is beyond the scope of this study, but we note sizeable differences between H_2L^{C2} and H_2L^C, in particular large deviations from the statistical differences for the former, which points to the presence of intra- or possibly intermolecular interactions. In particular, hydrogen bonding takes place between the pyridinium proton and either the carboxylate or imidazolium groups in the protonated subunits of the ditopic ligands. The presence of the poly(oxyethylene) pendant arms on the pyridine units may influence the energy barrier for the *trans*/*cis* conformational change needed for formation of these bonds considerably, thereby affecting the pK_a values.

Helicate formation in water: Self-assembly of the $[Ln_2(L^{C2})_3]$ helicates in water was monitored by electrospray mass spectrometry for the lanthanides La, Eu, Gd, Tb and Lu by adding stoichiometric amounts of H_2L^{C2} (3×10^{-4} M) to the corresponding perchlorate in the presence of 10% acetonitrile to favor ionization. In all cases, only one series of main peaks, which corresponds to a parent species with overall formula $[Ln_2(L^{C2})_3]$, was detected (Table 1).

Table 1. Most abundant species in the ESI mass spectra of H_2L^{C2} (3×10^{-4} M) and of stoichiometric 2:3 (Ln:H_2L^{C2}) solutions (Ln = La, Eu, Gd, Tb, Lu). Solvent: water/acetonitrile (9/1 v/v).

	m/z (obs)	*m/z* (calc)	($\Delta m/z$) [ppm]	MW [Da][a]
$[H_2L^{C2}+H]^+$	843.3566	843.3559	9	2800.50
$[\{La_2(L^{C2})_3\}+2H]^{2+}$	1400.8818	1400.9139	23	2690.82
$[\{La_2(L^{C2})_3\}+H+Na]^{2+}$	1411.8406	1411.9049	46	–
$[\{La_2(L^{C2})_3\}+2Na]^{2+}$	1422.7963	1422.8555	42	–
$[\{Eu_2(L^{C2})_3\}+2Na]^{2+}$	1437.5366	1437.4164	84	2826.84
$[\{Gd_2(L^{C2})_3\}+2H]^{2+}$	1419.3853	1419.4265	29	2836.85
$[\{Gd_2(L^{C2})_3\}+2Na]^{2+}$	1441.3658	1441.4085	30	–
$[\{Tb_2(L^{C2})_3\}+2H]^{2+}$	1420.8291	1420.9321	72	2838.85
$[\{Tb_2(L^{C2})_3\}+H+Na]^{2+}$	1431.7574	1431.9231	116	–
$[\{Lu_2(L^{C2})_3\}+2H]^{2+}$	1436.9131	1436.9476	24	2870.88
$[\{Lu_2(L^{C2})_3\}+H+Na]^{2+}$	1447.8719	1447.9385	46	–

[a] Molecular weight of the helicate with formula $C_{129}H_{144}Ln_2N_{18}O_{36}$.

With few exceptions, the accuracy of the *m/z* values is in the range 20–50 ppm. In addition, the isotopic distributions of these peaks are in good agreement with the simulated ones, as shown in Figure 1. It is noteworthy that no species corresponding to other stoichiometries (e.g. 1:2, 1:3, 2:2, or 2:1) are observed, which indicates that the helicates are the major species in solution.

A ^{1}H NMR titration of H_2L^{C2} (10^{-3} M) with lutetium(III) perchlorate was conducted in [D_{11}]tris/DCl buffer (0.1 M in D_2O; pD 7.8, tris = trishydroxymethylaminomethane) up to an $[Lu^{III}]_t/[H_2L^{C2}]_t$ ratio (*R*) of 2. The signals of the unbound ligand are broadened, especially in the aromatic range, which reflects a slow conformational exchange on the NMR timescale between at least two conformations of the ligand, as indicated by the observation of two signals for the methylene bridge at $\delta = 3.75$ and 3.85 ppm. Addition of the Lu^{III} salt results in the appearance of sharp signals concomitant with a complete disappearance of the ligand resonances (at $R = 0.66$). Further addition of Lu^{III} does not modify the spectrum, which is in line with the formation of a single main triple-stranded helical species in solution with appreciable stability (Figure S3 in the Supporting Information). The pyridine protons of the helicate are shielded, as expected, owing to coordination to the metal ion, and a large chemical shift difference (0.47 ppm) is also observed for the nitrogen-bound methyl group of the imidazole units. The terminal methoxy groups ($\delta = 3.13$ ppm) and the methylene bridge ($\delta = 4.08$ ppm) appear as one singlet each, which is consistent with three equivalent ligand strands.

The interaction of Ln^{III} (Ln = La, Eu, Lu) with H_2L^{C2} was quantified by spectrophotometric titrations of the ligand (10^{-5} M) with lanthanide perchlorate solutions (5×10^{-3} M) up to a total concentration ratio *R* of 4 and at pH 7.4. The UV-vis spectra display well-defined isosbestic points at 318, 262, and 247 nm (Figure 2, top) and an evolving factor analysis points to the presence of four absorbing species. Several models were tested, but the data were best fitted by non-linear least-squares techniques to the following set of equa-

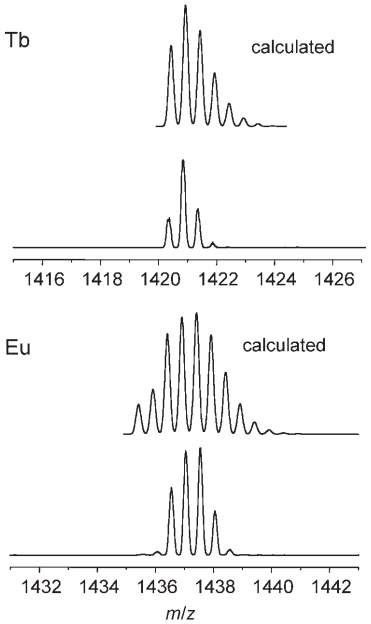

Figure 1. Parts of the electrospray mass spectra of solutions containing a 2:3 stoichiometric mixture of Ln^{III} and H_2L^{C2} in water/acetonitrile (9/1, v/v). Ln = Eu (bottom) and Tb (top). The calculated spectra are shown above the experimental data. $[H_2L^{C2}]_t = 3\times10^{-4}$ M.

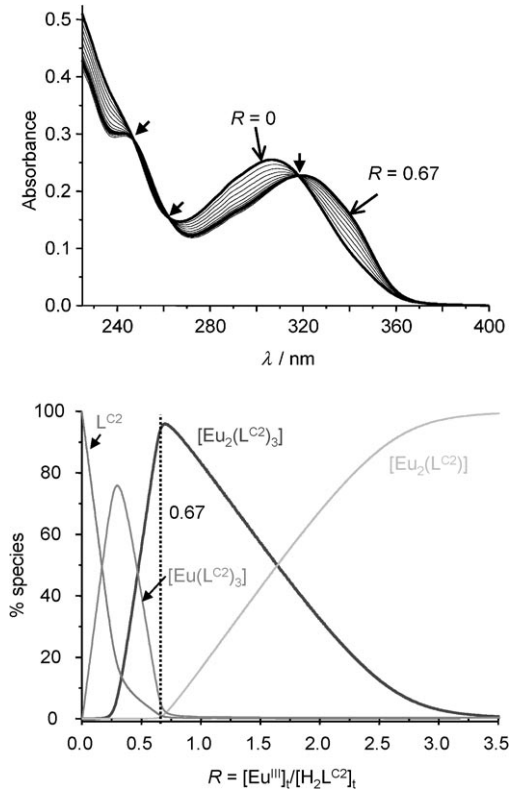

Figure 2. Top: Analysis, by using UV-vis spectroscopy, of the titration of H_2L^{C2} 10^{-5} M with $La(ClO_4)_3{\cdot}xH_2O$ at pH 7.4 (Tris-HCl 0.1 M) and 298 K; $R = [La^{III}]_t/[H_2L^{C2}]_t$; the small arrows denote isosbestic points. Bottom: Distribution diagram for Eu^{III} ($[H_2L^{C2}]_t = 10^{-4}$ M) drawn with the conditional stability constants reported in Table 2.

tions [Eqs. (6–8)](protons and charges have been omitted for clarity):

$$3L^{C2} + Ln \rightleftharpoons [Ln(L^{C2})_3] \qquad \log\beta_{13} \qquad (6)$$

$$3L^{C2} + 2Ln \rightleftharpoons [Ln_2(L^{C2})_3] \qquad \log\beta_{23} \qquad (7)$$

$$L^{C2} + 2Ln \rightleftharpoons [Ln_2(L^{C2})] \qquad \log\beta_{21} \qquad (8)$$

The residuals were calculated to be 2.3×10^{-4} for La, 7.6×10^{-4} for Eu and 4.6×10^{-4} for Lu. The recalculated spectra are strongly correlated (Figure S4 in the Supporting Information), which means that the conditional constants collected in Table 2 have to be considered with some care. There is little variation in these constants on going from La to Lu, except for a slightly larger stability of the 2:3 helicate with Lu^{III}. This is not the case for H_2L^C, however, for which the lanthanum helicate is significantly more stable. In summary, the introduction of the poly(oxyethylene) substituents in H_2L^{C2} does not affect the stability of the helical structures with the ions in the middle and at the end of the Ln^{III} series appreciably. The speciation diagram (Figure 2, bottom) shows that the main species at a total ligand concentration of 10^{-4} M is the helicate (95%), with the other two metal complexes accounting for about 5% of the total species in equilibrium. There is a negligible concentration of both free ligand and Eu^{III}. When the total ligand concentration reaches the millimolar range, the helicate represents more than 98% of the species in solution. These findings are consistent with the ESI-MS and NMR spectroscopic data reported above and suggest that 2:3 solutions are appropriate for bioanalyses since the complex concentrations used for the cell-staining experiments described below are in the range 2.5×10^{-5} to 5×10^{-4} M (total ligand concentrations: 7.5×10^{-5} to 1.5×10^{-3} M).

Table 2. Conditional stability constants (pH 7.4, Tris-HCl 0.1 M; 298 K) for the systems Ln/H_2L^{C2} compared to $\log\beta_{23}$ for Ln/H_2L^C (data taken from ref.[47]). Standard deviations are given in parentheses.

L	Constant	La	Eu	Lu
L^{C2}	$\log\beta_{13}$	18.8(2)	18.1(2)	18.7(3)
	$\log\beta_{23}$	24.9(4)	25.5(4)	26.3(4)
	$\log\beta_{21}$	11.7(3)	11.8(5)	12.4(2)
L^C	$\log\beta_{23}$	30(1)	26.1(4)	27.3(6)

Photophysical properties: The uncomplexed hexadentate receptor displays a main absorption band centered at 307 nm ($\log\varepsilon=4.54$) in addition to a shoulder at around 243 nm ($\log\varepsilon=4.58$) at pH 7.4. According to CACheⓇ calculation, these bands arise from $\pi\rightarrow\pi^*$ transitions involving intramolecular electron transfer from the benzimidazole units to the pyridine and carboxylic acid groups. Complexation to Ln^{III} ions induces a bathochromic shift of about 15 nm to 320–324 nm depending on the metal ion (see Figure S4 in the Supporting Information). The 2:3 species has quite a large molar absorption coefficient ($\log\varepsilon=4.93$), which is a definite advantage for an analytical probe.

Excitation into the lowest energy band results in emission from the ligand singlet state, which is observed in the form of a structured band with two maxima at 384 (0-phonon transition) and 404 nm; this band undergoes a slight red shift (4–8 nm) upon complexation. An additional emission band, which extends up to 650 nm, is observed under time-resolved conditions at 77 K. This band displays an extended vibronic fine structure with an average spacing of about 1400–1500 cm^{-1}, which corresponds to a ring breathing mode. The maximum is located at 489 nm and the 0-phonon transition at 434 nm (Figure 3), while the corresponding lifetime is 1280 ± 125 ms. The latter transition undergoes a red shift to 457 nm in the 2:3 helicates with non-luminescent metal ions (see Figure S5 in the Supporting Information), while the lifetime is reduced to about 620 ms for the compounds with La^{III} and Lu^{III} and to 8.7 ms for Gd^{III}. The efficacy of the intersystem crossing to the triplet state is very low for the unbound ligand; the heavy-atom effect is small for the La^{III} and Lu^{III} helicates (ratio $I(^3\pi\pi^*)/I(^1\pi\pi^*)\approx0.4$ and 0.3, respectively) but substantial for Gd^{III}, for which the $^3\pi\pi^*$ emission is by far the largest ($I(^3\pi\pi^*)/I(^1\pi\pi^*)\approx6$).

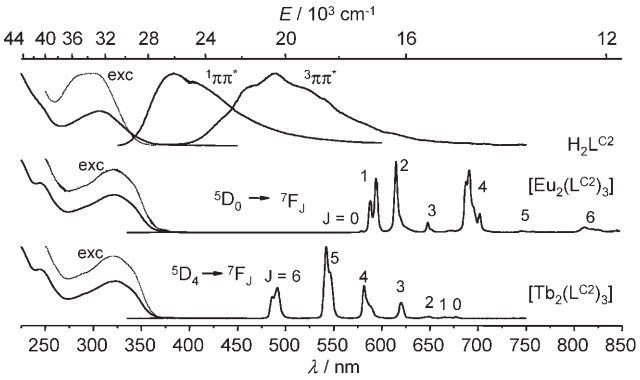

Figure 3. Left: Absorption (——) and excitation (exc, •••••) spectra of 4.5×10^{-5} M H_2L^{C2} and 1.5×10^{-5} M $[Ln_2(L^{C2})_3]$. Right: The corresponding emission spectra upon excitation at 307–323 nm. All spectra were recorded at 295 K, except the $^3\pi\pi^*$ emission spectrum (77 K).

The ligand H_2L^{C2} sensitizes the luminescence of several lanthanide ions at room temperature, with emission in either the visible or near-infrared ranges. The best sensitization is obtained for Eu^{III} and Tb^{III}, for which the proportion of ligand fluorescence in the total emission spectrum is less than 1 and 2%, respectively. The metal-centered luminescence is sizeable for Sm^{III} (see Figure S6 in the Supporting Information), accounting for 64% of the total emission, while only faint Ln^{III}-centered emission is seen for Pr^{III} ($^3P_0\rightarrow{}^3F_2$, $^3H_6$, 610 nm), Dy^{III} ($^4F_{9/2}\rightarrow{}^6H_{13/2}$, $^6H_{15/2}$, 480, 575 nm) and Ho^{III} ($^5F_5\rightarrow{}^5H_8$, 650 nm) and none for Tm^{III} (see Figure S7 in the Supporting Information). Bands characteristic of Pr^{III} ($^1D_2\rightarrow{}^3F_4$: 1.03 μm), Nd^{III} ($^4F_{3/2}\rightarrow{}^4I_{9/2}$, $^4I_{11/2}$

and $^4I_{13/2}$: 0.89, 1.06 and 1.35 μm respectively), Sm^{III} ($^4G_{5/2}\rightarrow$ $^6H_{15/2}$, $^6F_{5/2}$ and $^6F_{7/2}$: 0.88, 0.94 and 1.04 μm), Eu^{III} ($^5D_0\rightarrow^7F_5$ and $^7F_6$: 0.75 and 0.83 μm, respectively), Ho^{III} ($^5F_5\rightarrow^5I_7$: 0.99 μm) and Yb^{III} ($^2F_{5/2}\rightarrow^7F_{7/2}$: 0.98 μm) are detected in the NIR range, while the $^4I_{13/2}\rightarrow^4I_{15/2}$ transition of Er^{III} at 1.54 μm is only seen in deuterated water.

The Eu^{III} emission spectrum can be interpreted as arising from a major species having identical chemical environments for the two Eu^{III} ions with pseudo-D_3 symmetry, as inferred from the high-resolution spectrum of a frozen solution of $[Eu_2(L^{C2})_3]$ in H_2O/glycerol (9/1, v/v) shown in Figure 4. The $^5D_0\rightarrow^7F_0$ transition is faint and rather symmetrical, with a width at half height of 17 cm^{-1}. The energy of this transition is 17234 cm^{-1} at 295 K. Using a known equation[52] and nephelauxetic parameters ($\delta_{carb}=-17.2$ cm^{-1} for the carboxylate and $\delta_{bzp}=-15.3$ cm^{-1} for heterocyclic nitrogen atoms)[53] gives a $\tilde{\nu}_{calc}$ value of 17231 cm^{-1}, which is quite close to the experimental value. The $^5D_0\rightarrow^7F_1$ transition displays a sharp component corresponding to a transition to the $^7F_1(A_1)$ sub-level and a second transition terminating on the split $^7F_1(E)$ level. The A_1–E separation (161 cm^{-1}) reflects the strength of the crystal field (B^2_0 crystal-field parameter of approximately -600 cm^{-1}), while the splitting of the E level (31 cm^{-1}) is a measure of the distortion from D_3 symmetry.[54] The data for helicates with H_2L^C (at 295 K) and H_2L^{C3} (at 295 K)[49] are $\Delta E(A_1\text{–}E)=171$ and 164 cm^{-1} and $\Delta E(E\text{–}E)=28$ and 42 cm^{-1}, respectively. Taking this distortion into account, the other features of the spectrum are in line with group-theoretical predictions for D_3 symmetry

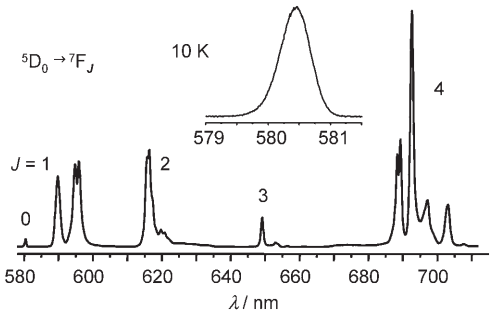

Figure 4. High-resolution luminescence spectrum of a stoichiometric 2:3 solution (Eu^{III}:H_2L^{C2}) in water/glycerol (9/1, v/v) at 10 K, under ligand excitation (341 nm)($[Eu_2(L^{C2})_3]=10^{-4}$ M; $[H_2L^{C2}]_t=3\times10^{-4}$ M).

The luminescence decays measured for all the emitting ions are single exponential functions. The corresponding lifetimes are collected in Table 3 along with the hydration numbers calculated from known phenomenological equations for Nd^{III}, Eu^{III}, Tb^{III} and Yb^{III}.[55–57] A hydration number of almost zero is estimated in each case, which means that the overall luminescence data clearly indicate that the chemical environment of the two Eu^{III} ions in $[Eu_2(L^{C2})_3]$ is very close to that evidenced by X-ray crystallography for the helicate with H_2L^C.[47]

Table 3. Lifetimes (at room temperature), hydration numbers and quantum yields upon ligand excitation (323 and 355 nm) of stoichiometric 2:3 solutions (Eu^{III}:H_2L^{C2}) at 295 K, pH 7.4 and with $[H_2L^{C2}]_t=4.5\times10^{-5}$ M (10^{-4} M for Nd^{III}). Data for the Eu^{III} and Tb^{III} helicates with H_2L^C and H_2L^{C3} are also given for comparison.

Ln	$\tau(H_2O)$ [μs]	$\tau(D_2O)$ [μs]	q	Q^{Ln}_L [%]
Nd	0.21 ± 0.02	1.28 ± 0.01	0.1	0.031 ± 0.006
Sm	30.4 ± 0.4	163 ± 3	[a]	0.38 ± 0.06
Eu	2430 ± 90	4380 ± 40	−0.1	21 ± 2
[b]	2430 ± 10	4660 ± 20	0.2	24 ± 2
[c]	2200 ± 100	4000 ± 100	0	11 ± 1
Tb	650 ± 20	940 ± 20	[d]	11 ± 2
[b]	50 ± 5	[a]	[d]	1.2 ± 0.2
[c]	390 ± 40	1400 ± 100	[d]	0.34 ± 0.04
Dy	0.16 ± 0.01	0.26 ± 0.1	[a]	[a]
Yb	4.40 ± 0.07	49.3 ± 0.8	0.0	0.15 ± 0.03

[a] Not determined. [b] Data for $[Ln_2(L^C)_3]$.[47] [c] Data for the main species $[Ln_2(L^{C3})_3]$.[48] [d] Equation not applicable (see text).

As far as the hydration numbers are concerned, we note that the usual phenomenological equations are not applicable to Tb^{III} in our case because one of the basic hypotheses is not met, namely that quenching by OH vibrations is the only main non-radiative deactivation process. Although far less important than for the helicates with H_2L^C[47] and H_2L^{C3},[49] some back-transfer is operating, which explains the relatively short lifetime of the Tb($^5D_4$) level. This lifetime is temperature dependent, reaching 2.58 ± 0.05 ms in H_2O and 2.67 ± 0.04 ms in D_2O at 77 K. The latter figure allows a q value of around −0.2 to be estimated at this temperature, which is in line with the other hydration numbers. The Tb($^5D_4$) lifetime versus temperature plot presents a discontinuity at around 240 K upon cooling, which points to a probable phase transition occurring at this temperature. However, this discontinuity is attenuated upon heating from 10 K to room temperature, and analysis of the data (see Figure S8 in the Supporting Information) yields an activation energy of 1600–1800 cm^{-1}. This range corresponds to C=O and C=C vibrations in the IR spectrum and is in line with a vibration-assisted energy back-transfer process operating in this helicate.

Stability of the Eu^{III} helicate: The stability constants reported above are consistent with those published for similar systems. However, since the spectra of the various species in equilibrium are strongly correlated, we turned to luminescence to check the relative stability of the Eu^{III} helicate with respect to a known polyaminocarboxylate, namely ethylenediamine tetraacetate (edta; $\log K(Eu)=17.3$[58]). The emission intensity of a 2:3 (Eu^{III}:H_2L^{C2}) solution was monitored for 28 days after initial addition of 15 equivalents of edta ($t=0$) and a further 85 equivalents after 44 h. The emission and excitation spectra of $[Eu(edta)(H_2O)_n]^-$ ($n=3$, according to lifetime measurements) and $[Eu_2(L^{C2})_3]$ are quite different (see Figure S9 in the Supporting Information), although no change was observed in either the overall emission intensity or the intensity ratios $I(^5D_0\rightarrow^7F_J)/I(^5D_0\rightarrow^7F_1)=^7F_J/^7F_1$ ($J=0$–4; see Table S1 in the Supporting Infor-

mation). Similarly, H_2L^{C2} was added in 2:3 stoichiometry to an initial solution of $[Eu(edta)(H_2O)_n]^-$ (3×10^{-5} M; Figure 5). This latter complex is not luminescent upon excitation at 323 nm and the rise in the luminescence intensity was monitored with time at both 615 ($^5D_0\rightarrow{}^7F_2$) and 691 nm ($^5D_0\rightarrow{}^7F_4$; cf. Figure 4); the "recovery" of the total luminescence was 75.5% of the expected intensity after 12 h and more than 92% after 21 days.

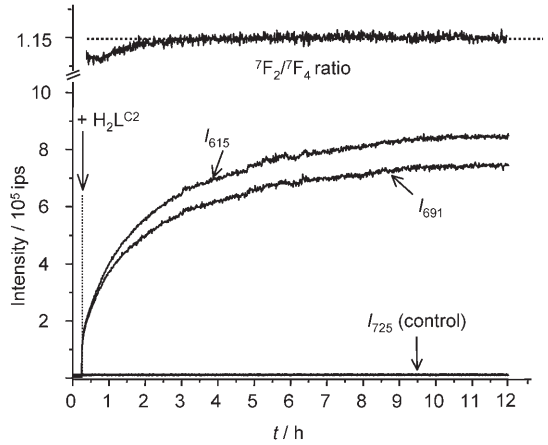

Figure 5. The increase in luminescence intensity (bottom) and the $^7F_4/^7F_2$ ratio (top) against time, after adding 4.5×10^{-5} M H_2L^{C2} to a 3.0×10^{-5} M solution of $[Eu(edta)(H_2O)_n]^-$.

Some dissociation of the helicate is observed if edta is replaced by 100 equivalents of diethylenetrinitrilo pentaacetate (dtpa; $\log K(Eu)=22.4$[58]): the luminescence intensity drops by about 10% after 24 h and 20% after 30 days, with a concomitant increase in the ligand singlet-state emission from 0.5% of the total luminescence (in the absence of dtpa) to 5%. The helicate also forms upon addition of H_2L^{C2} to the dtpa complex, although to a lesser extent than with edta. Since living media contain anions and cations which may compete for the Ln^{III} ion (exchange reactions) or for the ligand (transmetalation), we checked the impact of citrate and L-ascorbate (which may quench Ln excited states)[15] on the luminescent properties of the Eu^{III} helicate; no loss in luminescence was recorded four days after addition of 100 equivalents (1.5×10^{-3} M) of either of these anions. On the other hand, a small decrease in intensity (approx. 5%) was noted 12 h after adding 10 equivalents of zinc (150 μM); this concentration is, however, well above that found in blood plasma (5–15 μM). These experiments clearly point to the Eu^{III} helicate having a larger stability than the chelate with edta and a comparable stability to the dtpa complex, while resisting ligand exchange and transmetalation reactions with analytes commonly found in living cells.

Cell-imaging properties: We will now demonstrate the potentiality of the $[Ln_2(L^{C2})_3]$ helicates as cell-staining agents on the human cervical carcinoma cell line HeLa. We have shown in a preliminary communication[49] that incubation of these cells with up to 500 μM of helicate at 37°C during 24 h does not affect their viability. The data collected in Table 4 and Figure S10 in the Supporting Information confirm that this is also the case for other cell types.

Table 4. Cell viability values [%] as determined from the WST-1 test after incubation for 24 h at 37°C in the presence of various concentrations of $[Eu_2(L^{C2})_3]$.

Conc [μM]	Jurkat	5D10	MCF-7	HeLa
0	100	100	100	100
125	92±16	93±11	92±13	88±3
250	101±4	99±1	102±7	101±1
500	107±4	89±4	101±1	108±2

Luminescence microscopy was carried out with an optimized set-up for monitoring the intake and localization of the $[Ln_2(L^{C2})_3]$ (Ln = Sm, Eu, Tb) helicates. In particular, excitation at 330 nm combined with appropriate excitation and emission filters (see Figures S11 and S12 in the Supporting Information) yielded bright images even for an incubation concentration of the Eu^{III} helicate as low as 10 μM. In the case of Tb^{III}, bright images were obtained on the luminescence microscope with a loading concentration of 125 μM and a specific bandpass filter of 35 nm ($^5D_4\rightarrow{}^7F_5$ transition). Images were also obtained with Sm^{III} despite its low quantum yield (0.38%), albeit at the cost of a higher helicate incubation concentration (250 μM) and longer incubation time (24 h; Figure 6). Owing to the large molar absorption coefficient for the maximum ligand absorption at 323 nm, enough absorbance is left at 405 nm to acquire images with a confocal microscope at this excitation wavelength (Figure 7, bottom).

The helicates stain the cytoplasm of the cells, as shown by the luminescence being associated with distinct internal structures, which suggests a specific organelle localization. Confirmation of the localization of $[Eu_2(L^{C2})_3]$ in the cyto-

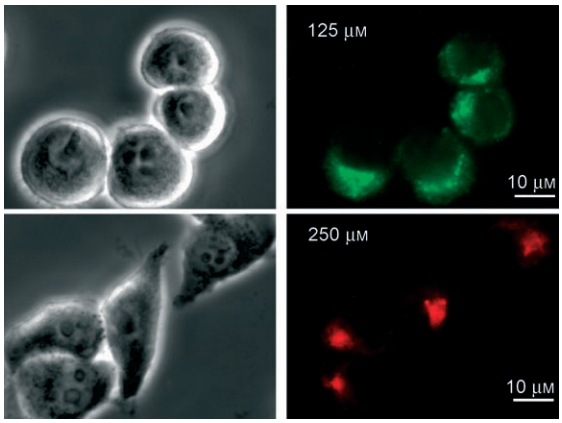

Figure 6. Images of HeLa cells obtained upon excitation at 330 nm and with an exposure time of 60 s with $[Tb_2(L^{C2})_3]$ (top; 7 h incubation, emission BP 545) and $[Sm_2(L^{C2})_3]$ (bottom; 24 h incubation, emission filter LP 585).

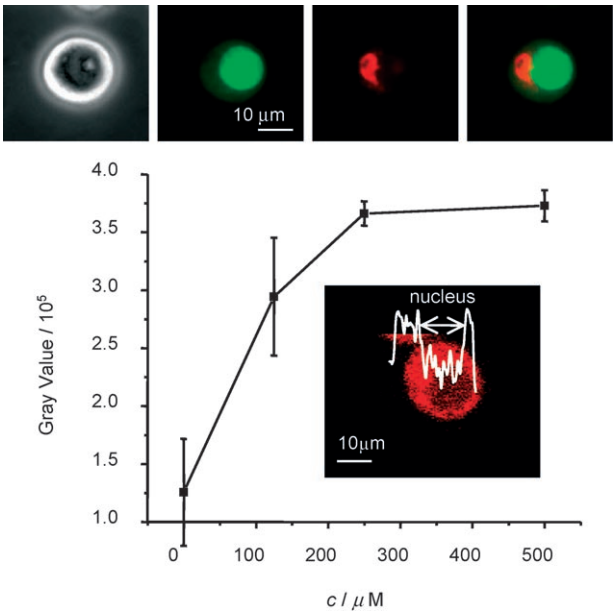

Figure 7. Top: Counterstaining experiment with acridine orange (AO); $\lambda_{ex}=330$ nm, exposure time of 10 s for Eu^{III}; $\lambda_{ex}=470$ nm, exposure time of 30 ms for AO. Bottom: Intensity of Eu^{III} luminescence versus incubation concentration $[Eu_2(L^{C2})_3]$ as measured by using a confocal microscope. Inset: a densitometry measurement across a cell showing the cytoplasmic localization of the helicate.

plasm came from counterstaining experiments. Thus, live cells were loaded with the $[Eu_2(L^{C2})_3]$ helicate (250 μM in RPMI-1640, 5 h at 37 °C) and then incubated with 100 μg mL^{-1} of the commercially available nucleus stain acridine orange (5 min at room temp.) and examined using appropriate filters (Figure 7): the red Eu^{III} emission is clearly seen in the cytoplasm of the cells while the green acridine orange emission originates from the cell nucleus. Additionally, a densitometric analysis across one cell performed with a confocal microscope also clearly points to the helicate being present in the cytoplasm.

In order to determine the mechanism by which the cells take up the helicates and their subsequent localization within the cytoplasm, the time course and temperature-dependence of the complex loading were determined (Figures S13–S15 in the Supporting Information). The first bright spots in the cytoplasm of the cells can be observed as early as 15 min after incubation with the complex. No Eu^{III} luminescence was observed when the complex was loaded at 4 °C, thus indicating that the helicate is likely to enter the cells by endocytosis. Initial experiments performed under non-optimum conditions seemed to indicate the presence of an active uptake mechanism,[49] however the present experiments, which were carried out several times under optimized experimental conditions, provide unambiguous results. These findings were further confirmed in co-localization experiments in which live cells were loaded simultaneously with the Eu^{III} helicate and commercially available BIODIPY FL labeled transferrin, which is a known marker of recycling endosomes,[59] or LDL, which is a marker for late endosomes and lysosomes.[60] Cell uptake of transferrin and LDL is a well-established receptor-mediated process. HeLa cells were incubated with the $[Eu_2(L^{C2})_3]$ helicate and the organic marker and imaged by luminescence microscopy using appropriate filters (see Figure 8 and Figure S16 in the Supporting Information). The vast majority of compartments which internalized the Eu^{III} helicate also contained BIODIPY FL labeled LDL or transferrin (Figure 8, third column), as evidenced by the appearance of bright yellow spots (Figure 8, fourth column) after merging the images, and nearly all the endocytosed Eu^{III} helicate is internalized in receptor-containing vesicles. These observations strongly suggest the uptake of the complex by a lysosomally directed and/or a recycling endosomal pathway.

Helicate concentration in HeLa cells: The intracellular concentration of the Eu^{III} complex was measured in a given cell cohort using the DELFIA® technique. Thus, cells were loaded overnight with a 25 μM solution of the Eu^{III} helicate in a six-well cell-culture plate and harvested by trypsinisation after extensive washing with PBS. The number of labeled cells was estimated by staining with trypan blue. The Eu^{III} luminescence was measured after complete cell lysis (Figure S17 in the Supporting Information). Each cell contains, on average, 7.9×10^{-16} mol of $[Eu_2(L^{C2})_3]$. Taking into account a cell volume of between 2.6×10^3 and 4.2×10^3 μm^3, as estimated from the cell diameters measured under the optical microscope, this translates into an intracellular con-

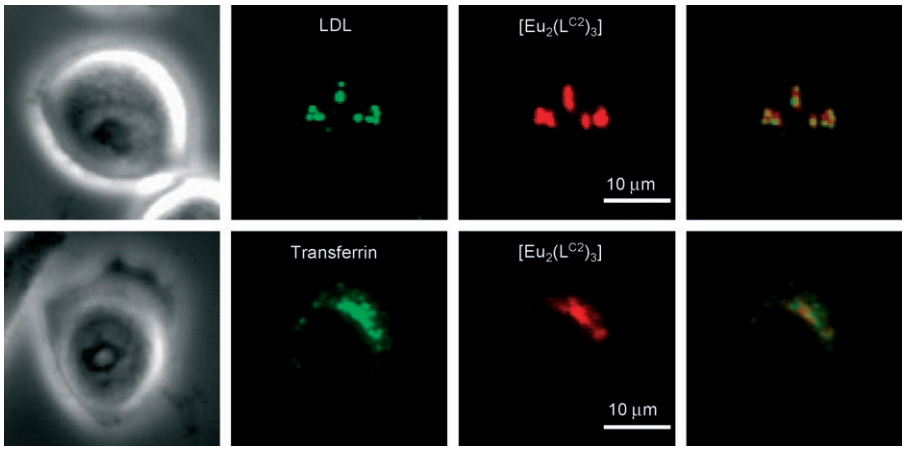

Figure 8. Co-localization of cells loaded with 250 μM $[Eu_2(L^{C2})]$ and 15 μg mL^{-1} BIODIPY FL LDL (0.5 h, top) or 50 μg mL^{-1} Transferrin (2 h, bottom). First column: bright field images. Second column: BIODIPY FL labeled LDL ($\lambda_{exc}=470$ nm, 1 s exposure time) or Transferrin fluorescence ($\lambda_{exc}=470$ nm, 2 s exposure time). Third column: Eu^{III} luminescence ($\lambda_{exc}=365$ nm, 30 s exposure time). Fourth column: merged images.

centration of between 0.18 and 0.30 μM (assuming $d=1$), which is about the same as that found for a cyclen-based luminescent stain.[28]

We also checked that the helicates survive unchanged in the cells by measuring their photophysical properties after internalization. The overall shape of the emission spectra for Eu^{III}[49] and Tb^{III} (Figure 9, middle), the profile of the

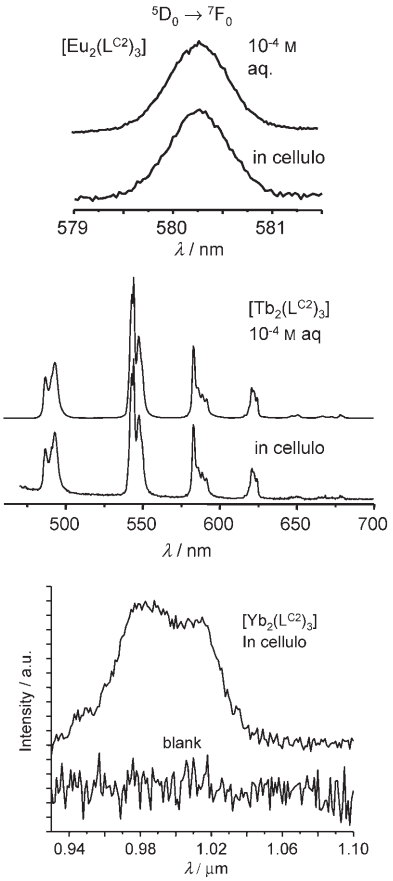

Figure 9. A comparison of the emission spectra of $[Ln_2(L^{C2})_3]$ in water (10^{-4} M; pH 7.4; $\lambda_{exc}=330$ nm) and in cellulo (HeLa cells; initial concentration: 125 μM; incubation time: 15 h, 37 °C). Ln = Eu (top), Tb (middle) $^5D_0 \rightarrow {}^7F_0$ transition, Yb (bottom)(initial concentration: 250 μM; incubation time: 24 h, 37 °C). $\lambda_{exc}=330$ nm/Bp = 14 nm; $\lambda_{emi}=930$–1100 nm/Bp = 14 nm (spectra not corrected); integration time $\tau=1$ s.

$Eu(^5D_0 \rightarrow {}^7F_0)$ transition (Figure 9, top) and the relative intensities of the $^5D_J \rightarrow {}^7F_{J'}$ transitions (Table S2 in the Supporting Information) are indeed identical to those found for the aqueous solutions. Some differences, however, are observed for the lifetimes of the excited levels. In the case of $Eu(^5D_0)$, a single exponential decay is measured with an associated lifetime of 1.6 ± 0.2 ms, while Tb^{III} solutions in cellulo present a biexponential decay with associated lifetimes of the $Tb(^5D_4)$ excited state of 0.65 ± 0.02 ms (55 %), which corresponds to the lifetime measured in solution at pH 7.4, and 0.25 ± 0.01 ms (45 %), which is much shorter than that of the aqua ion (0.457 ms).[61] These phenomena may be a result of quenching by endogenous antioxidants[15] and will be studied in more detail in the near future.

Another very encouraging result is the observation of in cellulo Yb^{III} emission after incubating HeLa cells 24 h at 37 °C with a 250 μM solution (Figure 9, bottom; cf. Figure S7 in the Supporting Information). The corresponding lifetime is 4.3 ± 0.1 μs, which is perfectly in line with the value found for an aqueous solution (Table 3).

Discussion and Conclusions

The chemical rules guiding the cellular uptake characteristics of Ln^{III} complexes are not yet known, and prediction of cellular localization is difficult because it depends on several parameters, including chemical structure, bulkiness, hydrophobicity and the overall charge of the metal chelate. From the limited amount of literature data available, it seems, however, that there is a tendency for neutral, high molecular weight metal complexes to be internalized in living cells by endocytosis while an active mechanism is operative for low molecular weight, negatively charged chelates. This was demonstrated for the first time by the uptake of d-transition metal complexes, namely iron complexes, by epithelial cells, in which neutral complexes with high molecular weight ligands (e.g. dextran) were taken up by endocytosis and retained in phagosomes whereas the internalization of complexes with low molecular weight ligands, such as 8-hydroxyquinoline, was much faster.[62]

A similar trend is observed for lanthanide complexes, with positively charged, low molecular weight, cyclen-based complexes being taken up by the cells by an active mechanism and being preferentially localized in the nucleus of living cells.[28,29,63–65] The microscopy images in these latter reports show the migration of the complexes through the cytoplasm, across the nuclear membrane and into the nucleus, and show substructures within the nucleus. In these examples, the homing-in to the nucleus and localization in specific organelles such as mitochondria, which possess a negative surface potential and contain DNA, could be a result of the positive charge of these cyclen-based chelates. The class of luminescent stains described herein enters into the cells by endocytosis, as shown by co-localization and temperature-dependence experiments, therefore interaction with specific cellular organelles will only be possible if the helicates are able to escape from the endosomes. It is known that arginine-rich cell penetrating peptides (AR-CPPs) can increase cellular uptake and the potential of endosomal escape, and the effect of coupling AR-CPPs to functionalized helicates on their subsequent cellular uptake and possible endosomal escape is under evaluation.[66]

The bimetallic luminescent probe system described herein displays interesting sensitization properties. In the case of Eu^{III}, the intrinsic quantum yield (i.e. the quantum yield upon direct metal excitation), which reflects the deactivation processes operating in the helicate, can be calculated from the observed and radiative lifetimes. The latter, which can

be estimated by a known procedure,[67] is 6.9 ms for $[Eu_2(L^{C2})_3]$ as compared to 6.2 ms for $[Eu_2(L^{C3})_3]$[48] and 7.1 ms for $[Eu_2(L^{C})_3]$.[47] This, in turn, leads to intrinsic quantum yields of 36.4, 35.7 and 36.7%, respectively. In other words, substitution of poly(oxyethylene) pendants at either the benzimidazole or pyridine positions does not affect the deactivation processes despite the greater flexibility of the ligand strands. On the other hand, the overall quantum yields (Q^{Ln}_L) of the Eu^{III} helicates are clearly affected, decreasing from 24% for helicates with H_2L^C to 21% and 11% for helicates with H_2L^{C2}, and H_2L^{C3}, respectively, which means that the sensitization efficacy (η_{sens}) provided by these ligands decreases in the sequence 67%, 58% and 30%, respectively. This is a remarkable electronic tuning of the photophysical properties of the helicates despite their very similar ligand-centered photophysical properties (see Figure S5 in the Supporting Information for a comparison between H_2L^{C2} and H_2L^{C3}). An even more dramatic effect is found for the helicates with Tb^{III}, an ion which is easily amenable to back-transfer processes. The overall quantum yield increases dramatically for $[Tb_2(L^{C2})_3]$ (see Table 3) compared to helicates with the other ligands, by factors of about 10 (H_2L^C)[47] and 33 (H_2L^{C3}).[48] The difference observed between the helicates with H_2L^C and H_2L^{C2} is consistent with the increase in the Tb($^5D_4$) lifetime from 0.05 to 0.65 ms and means that the main factor here is the back-transfer process, which is more efficient in the unsubstituted helicate. The increase in quantum yield from $[Tb_2(L^{C3})_3]$ to $[Tb_2(L^{C2})_3]$, on the other hand, cannot be explained similarly since the lifetime increases by a factor of only 1.7. It is noteworthy that if the efficiency of the intersystem crossing, as estimated from the relative triplet to singlet emission intensity ratios at 77 K, does not vary substantially between either the two unbound ligands (factor of about 1.7 in favor of H_2L^{C2}) or between their complexes with La^{III} and Lu^{III} (no variation), it increases by a factor of 4.5 in favor of H_2L^{C2} in the Gd^{III} chelates. We also observe that the band envelope of the ligand singlet emission at room temperature (Figure 10) extends more towards the visible region in the case of H_2L^{C2} than H_2L^{C3}. This means that if the singlet state were also involved in the overall ligand-to-metal transfer, as has been demonstrated for some lanthanide complexes,[68] the transfer may be substantially enhanced in the former system. Altogether, and given the complexity of the ligand-to-metal energy-transfer processes, we think that the unusually large enhancement in Tb^{III} luminescence is owed to a combination of several factors that are a consequence of the connection of an oxygen atom at position 4 of the pyridine units in H_2L^{C2}, inducing small but significant changes in the ligand wavefunctions.

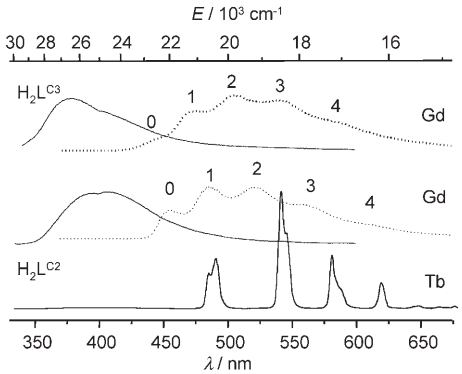

Figure 10. Comparison of ligand singlet (——, room temperature) and triplet (•••••, time-resolved conditions, 77 K) emission bands for $[Gd_2(L^{C2})_3]$ (bottom) and $[Gd_2(L^{C3})_3]$ (top). The emission spectrum of $[Tb_2(L^{C2})_3]$ is also plotted for comparison.

Given the high thermodynamic stability of the reported helicates, which makes them amenable to in vitro experiments, as well as their versatile and tunable photophysical properties, which results in their sensitization if bound to both visible (Sm^{III}, Eu^{III}, Tb^{III}) and near-infrared (Nd^{III}, Yb^{III}) emitting ions, the new class of bimetallic helical luminescent tags described here is certainly a valid multimodal alternative to the existing lanthanide chelates. The reported in cellulo Yb^{III} emission is a rare example[23] of such an NIR luminescence and opens wide perspectives for the design of in vivo NIR imaging probes. The sensitivity of the reported probes is high, as shown for the Eu^{III} helicate, which stains the cytoplasm of HeLa cells after only a few minutes of incubation at reasonably low concentrations. The molar absorption coefficient at the maximum of absorption is around 8.5×10^4 $M^{-1}cm^{-1}$, which means that εQ^{Ln}_L amounts to 323 (Sm^{III}), 17850 (Eu^{III}), 9350 (Tb^{III}) and 128 $M^{-1}cm^{-1}$ (Yb^{III}), the latter of which compares favorably to the xanthene-derivatized dota-based complexes recently evaluated for cell-imaging purposes, which have quantum yields of 7% (Eu^{III}) and 24% (Tb^{III}) with molar absorption coefficients at 336 nm of around 6000 $M^{-1}cm^{-1}$ and $\varepsilon\times Q^{Ln}_L$ values in the range 400–1500 $M^{-1}cm^{-1}$.[69] The only drawback of the described stains is the relatively low excitation wavelength needed (even if confocal images can also be obtained upon excitation at 405 nm), although this can potentially be overcome by two-photon excitation.

The class of luminescent stains described herein has two other fascinating features. One of these is chirality, which is an inherent property of the helicates and means that appropriate derivatization of the ligand should result in solutions enriched in one or the other (*P* or *M*) enantiomer. Secondly, the poly(oxyethylene) arms can be easily functionalized and we already have at hand several derivatives in which the terminal OMe group (Scheme 1) has been replaced by OH, CO_2H and NH_2 groups. Specific targeting experiments will be conducted with these derivatives as well as time-resolved imaging and in cellulo NIR detection.

Experimental Section

Starting materials and general procedures: Chemicals and solvents were purchased from Fluka A.G or Aldrich. Solvents were purified by passing them through activated alumina columns (Innovative Technology Inc. system).[70] Stock solutions of lanthanides were prepared just before use

in freshly boiled, doubly distilled water from the corresponding $Ln(ClO_4)_3 \cdot xH_2O$ salts (Ln = La, Lu, Gd, Tb, Eu; $x = 2.5$–4.5). These salts were prepared from their oxides (Rhône-Poulenc, 99.99%) in the usual way.[71] The concentrations of the solutions were determined by complexometric titrations using a standardized Na_2H_2EDTA solution in a urotropine buffered medium with xylenol orange as indicator.[72]

Analytical measurements: NMR spectra were recorded at 25°C with Bruker Avance DRX 400 (^{1}H: 400 MHz) and AV 600 (^{13}C: 99.8 MHz) spectrometers. The spectra of organic compounds were recorded for solutions in $CDCl_3$ (99.8%, Aldrich) or MeOD (99.8%, Aldrich) and those of the helicates for solutions in D_2O (99.9%, Aldrich) or NaOD (0.1 M starting from NaOD 25% from Aldrich (99.5%)); deuterated solvents were used as internal standards and chemical shifts are given with respect to TMS. The ESI mass spectra of the ligands were recorded with a Finningan SSQ 710C spectrometer using 10^{-5}–10^{-4} M solutions in acetonitrile/H_2O/acetic acid (50/50/1), with a capillary temperature of 200°C and an acceleration potential of 4.5 keV. The instrument was calibrated against the horse myoglobin standard and the analyses were conducted in positive mode. ESI-QTof mass spectra of the complexes were measured for solutions in water/acetonitrile (9/1 v/v) with a Q-Tof Ultima API mass spectrometer (Micromass, Manchester, UK) equipped with a Z-spray type ESI source. Phosphoric acid was used for the positive ion mass calibration range of 100–2000 m/z. Data were acquired and processed using Masslynx version 4.0. The electrospray conditions were as follows: capillary voltage: 2.3 kV; source temperature: 80°C; cone voltage: 35 V; source block temperature: 150°C. The ESI mobilization and drying gas was nitrogen. All experiments were performed in positive ion mode. The sample was introduced with a syringe pump at a rate of 20 $\mu L\,min^{-1}$. The spectra were simulated with Molecular Weight Calculator 6.42®. UV-visible spectra were measured for solutions in 0.2-cm quartz Suprasil® cuvettes with a Perkin–Elmer Lambda 900 spectrometer. Molecular modeling was performed with the CAChe® workpackage 7.5 (Fujitsu, 2000–2006). Protonation constants for H_2L^{C2} were determined with the help of a J&M diode array spectrometer (Tidas series) connected to an external computer. All titrations were performed in a thermostatted (25.0 ± 0.1°C) glass-jacketed vessel at $\mu = 0.1$ M (KCl). Stability constants were determined by titration of H_2L^{C2} with Ln^{III} (Ln = La, Eu, Lu) at fixed pH (7.4 in 0.1 M Tris-HCl buffer). Factor analysis[73] and mathematical treatment of the spectrophotometric data were performed with the Specfit® software.[74,75] IR spectra were recorded with a Spectrum One Perkin–Elmer FT-IR spectrometer equipped with an ATR accessory. Elemental analyses were performed at the Microchemical Laboratory of the University of Geneva.

The luminescence spectra and lifetimes were recorded with either a Horiba–Jobin Yvon FL 3-22 fluorimeter or a home-made high-resolution set-up, according to previously published procedures.[48,49,76] Quantum yields were measured by both a comparative method with $[Ln(dpa)_3]^{3-}$ as standard[77] and by an absolute method using an integration sphere, as described previously.[48] To demonstrate the consistency of the two methods, Table 5 gathers the results obtained for the Eu^{III} helicates, expressed in terms of quantum yields relative to $[Eu_2(L^C)_3]$.

Table 5. Relative quantum yields (reference: $[Eu_2(L^C)_3]$) obtained with the comparative method (left) and with the integration sphere (right).

	$Q_{f^6}^{Eu}$	$Q_{f^{62}}^{Eu}$	$Q_{f^{63}}^{Eu}$		$Q_{f^6}^{Eu}$	$Q_{f^{62}}^{Eu}$	$Q_{f^{63}}^{Eu}$
$Q_{f^6}^{Eu}$	1	1.10	2.14	$Q_{f^6}^{Eu}$	1	1.20	2.13
$Q_{f^{62}}^{Eu}$	0.91	1	1.94	$Q_{f^{62}}^{Eu}$	0.83	1	1.77
$Q_{f^{63}}^{Eu}$	0.47	0.52	1	$Q_{f^{63}}^{Eu}$	0.47	0.56	1

Diethyl 4-Hydroxypyridine-2,6-dicarboxylate (2): The synthesis of this compound was adapted from that described by Lamture et al.[78] Thus, chelidamic acid (**1**; 5 g, 27.3 mmol) was suspended in absolute ethanol (100 mL) and sulfuric acid (97%) was carefully added at room temperature with vigorous stirring. The yellow mixture was refluxed for 4 h and the solvents evaporated. Water (100 mL) was then added and the solvent evaporated again. The viscous residue was neutralized with a saturated solution of $NaHCO_3$ to pH 8 and the aqueous solution was extracted with CH_2Cl_2 (4 × 200 mL). The organic phase was dried with Na_2SO_4 and evaporated to give **2** as a pale solid, which solidified upon standing at room temperature (6.2 g, 95%). ^{1}H NMR (400 MHz, [D$_6$]DMSO): δ = 7.53 (s, 2H), 4.33 (q, ^3J = 7.13 Hz, 4H), 1.32 ppm (t, ^3J = 7.13 Hz, 6H). ESI-MS m/z calcd for $[M+H^+]$: 240.06; found 240.32.

Diethyl 4-{2-[2-(2-methoxyethoxy)ethoxy]ethoxy}pyridine-2,6-dicarboxylate (3): Triphenylphosphane (7.65 g, 29.2 mmol) and 2-[2-(2-methoxyethoxy)ethoxy]ethanol (4.8 g, 29.2 mmol) were added to a solution of **2** (3.5 g, 14.6 mmol) in thf (200 mL). DIAD (5.8 g, 29.2 mmol) was then slowly added whilst stirring and the solution was refluxed overnight. The solvent was evaporated, the crude product was added to 150 mL of 0.01 M NaOH and the solution was stirred 45 min, during which time white triphenylphosphanyl oxide precipitated. After filtration, the filtrate was extracted three times with 150 mL of CH_2Cl_2, the combined organic phases were dried over Na_2SO_4 and evaporated to give an oil, which was purified by chromatography (silica or neutral alumina, 100% ethyl acetate) to provide the desired product as an oil (4.0 g, 71%). ^{1}H NMR (400 MHz, $CDCl_3$): δ = 7.80 (s, 2H; H_{ar}), 4.47 (q, ^3J = 7.13 Hz, 4H; OCH_2-CH_3), 4.30 (td, ^3J = 4.75, ^4J = 1.08 Hz, 2H; H^1), 3.90 (td, ^3J = 4.75, ^4J = 1.08 Hz, 2H; H^2), 3.72 (td, ^3J = 5.3, ^4J = 2.6 Hz, 2H; $H^{3,4}$), 3.66–3.64 (m, 4H; $H^{3,4}$ and $H^{5,6}$), 3.53 (td, ^3J = 4.21, ^4J = 1.67 Hz, 2H; $H^{5,6}$), 3.37 (s, 3H; OCH_3), 1.38 ppm (t, ^3J = 7.13 Hz, 6H; OCH_2CH_3). ^{13}C NMR (600 MHz, $CDCl_3$): δ = 166.74 (C_{Ar}-O), 164.30 (C=O), 150.13 (C_{ar}), 114.36 (CH_{ar}),, 77.01 (OCH_2), 71.87 (OCH_2), 70.93 (OCH_2), 70.61 (OCH_2), 70.32 (OCH_2), 70.20 (OCH_2), 62.31 (OCH_2-CH_3), 58.95 (-CH_2-), 14.15 ppm (OCH_2-CH_3). ESI-MS m/z calcd for $[M+H^+]$: 386.17; found 386.36.

6-(Ethoxycarbonyl)-4-{2-[2-(2-methoxyethoxy)ethoxy]ethoxy}pyridine-2-carboxylic acid (4): Compound **3** (1.3 g, 3.37 mmol) was suspended in a solution of NaOH (54 mg, 0.4 equiv) in water (200 mL) and the solution was stirred for 2 h at room temperature. The evolution of the reaction was followed by TLC (silica plate, CH_2Cl_2/MeOH 97/3 v/v). After completion of the reaction, the basic aqueous solution was washed three times with 50 mL of CH_2Cl_2, acidified to pH 2.0 with 0.1 M HCl, and extracted four times with 50 mL of CH_2Cl_2. The combined organic phases were dried with Na_2SO_4 and evaporated to give **4** as an oil (0.65 g, 70%). ^{1}H NMR (400 MHz, $CDCl_3$): δ = 7.88 (s, 1H; H_{ar}), 7.85 (s, 1H; H_{ar}), 4.46 (q, ^3J = 7.14 Hz, 2H; OCH_2CH_3), 4.33 (t, ^3J = 4.75 Hz, 2H; H^1), 3.91 (t, ^3J = 4.75 Hz, 2H; H^2), 3.74 (d, ^3J = 6.0 Hz and d, ^3J = 5.3 Hz, 2H; $H^{3,4}$), 3.68–3.64 (m, 4H; $H^{3,4}$ and $H^{5,6}$), 3.54 (d, ^3J = 6.4 Hz and d, ^3J = 4.94 Hz, 2H; $H^{5,6}$), 3.37 (s, 3H; OCH_3), 1.38 ppm (t, ^3J = 7.14 Hz, 3H; OCH_2CH_3). ^{13}C NMR (600 MHz, $CDCl_3$): δ = 167.92 (C_{Ar}-O), 163.70 (C=O), 148.34 (C_{ar}), 148.18 (C_{ar}), 116.11 (CH_{ar}), 111.98 (CH_{ar}), 71.91 (OCH_2), 70.98 (OCH_2), 70,64 (OCH_2), 70.6 (OCH_2), 69.01 (OCH_2), 68.70 (OCH_2), 62.40 (OCH_2CH_3), 59.02 (CH_2), 14.21 (OCH_2CH_3). ESI-MS m/z calcd for $[M+H^+]$: 358.14; found 358.31.

Diester 6: Compound **4** (800 mg, 3.11 mmol), freshly distilled thionyl chloride (3.80 g, 31.1 mmol) and dmf (0.100 mL) were refluxed for 90 min in dry CH_2Cl_2 (120 mL) under an inert atmosphere. The pale solid formed after evaporation and pumping for 1 h was redissolved in 100 mL of dry CH_2Cl_2 and 2 mL of NEt_3. A solution of 3,3′-dinitro-4,4′-bis(*N*-methylamino)diphenylmethane (**5**; 283 mg, 1.2 mmol in 50 mL of CH_2Cl_2), which was synthesized according to a known procedure,[79] was then added dropwise. The resulting mixture was refluxed for 12 h under an inert atmosphere and the solvents were then evaporated. The orange residue was redissolved in CH_2Cl_2 (100 mL) and washed twice with 100 mL of half-saturated NH_4Cl solution. The combined organic phases were dried with Na_2SO_4, evaporated, and the resulting crude solid was purified by column chromatography (silica gel; CH_2Cl_2/MeOH, 100/0→98/2 v/v) to give **6** as an orange oil (535 mg, 60%). ^{1}H NMR (400 MHz, $CDCl_3$): δ = 8.04 (s, 2H; H_{py}), 7.79 (s, 2H; H_{py}), 7.68 (s, 2H; H_{ar}), 7.32 (s, 2H; H_{ar}), 6.98 (s, 2H; H_{ar}), 4.34 (m, 4H; H^1), 4.28 (q, ^3J = 5.18 Hz, 4H; OCH_2CH_3), 4.02 (s, 6H; NCH_3), 3.89 (m, 4H; H^2), 3.73 (m, 4H; $H^{3,4}$), 3.67 (m, 4H; $H^{3,4}$), 3.63 (m, 4H; $H^{5,6}$), 3.54 (m, 4H; $H^{5,6}$), 3.38 (s, 2H; CH_2), 3.35 (s, 6H; OCH_3), 1.35 ppm (t, ^3J = 5.18 Hz, 6H; OCH_2CH_3). ^{13}C NMR (600 MHz, $CDCl_3$): δ = 166.74 (C_{ar}-O), 164.03 (C=O), 153.78 (C_{ar}) , 147.77 (C_{ar}), 145.61 (C_{ar}), 139.52 (C_{ar}), 134.49 (C_{ar}), 131.45 (C_{ar}),

125.58 (CH_{ar}), 113.80 (CH_{ar}), 113.42 (CH_{ar}), 70.88 (OCH_2), 70.59 (OCH_2), 70.55 (OCH_2), 69.10 (OCH_2), 69.03 (OCH_2), 68.12 (OCH_2), 61.61 (OCH_2CH_3), 58.99 (OCH_3), 40.55 (CH_2), 38.55 (NCH_3), 14.20 ppm (OCH_2CH_3). ESI-MS m/z calcd for $[M+H^+]$: 995.38; found 995.33. calcd for $[M+2H^+]/2$: 498.20; found 498.37. calcd for $[M+Na^+]$: 1017.31; found 1017.33.

Diester 7: Freshly activated iron powder (0.87 g, 15.9 mmol) and HCl (37%; 4.4 mL, 44 mmol) were added to a solution of **6** (535 mg, 0.54 mmol) in ethanol/water (110/30 mL). The mixture was refluxed overnight under an inert atmosphere then the unreacted iron was filtered off after cooling and the solvents evaporated. The crude product was redissolved in ethanol, sulfuric acid was added carefully (2 mL) and the solution was refluxed overnight. It was then cooled and the solvents removed. Water (100 mL) was added and the pH was adjusted to 6 with a saturated aqueous solution of $NaHCO_3$. H_2Na_2EDTA was then added (20 equiv), and subsequent addition of 30% H_2O_2 (1 mL) resulted in a brown color. The pH was adjusted to 7 with a saturated aqueous solution of $NaHCO_3$ before extraction with two 250-mL portions of CH_2Cl_2. This procedure was repeated twice and the organic phases were combined and extracted again with a solution of H_2Na_2EDTA (20 equiv) in aqueous $NaHCO_3$. The pale brown crude product was collected after drying with Na_2SO_4, filtration and evaporation to dryness, and was purified by column chromatography (silica gel; CH_2Cl_2/MeOH, 100/0→97/3) to give a pale-yellow solid (220 mg, 45%). ^{1}H NMR (400 MHz, $CDCl_3$): $\delta=8.09$ (d, $^3J=2.27$ Hz 2H; H_{ar}), 7.71 (d, $^3J=2.27$ Hz, 2H; H_{ar}), 7.69 (s, 2H; H_{ar}), 7.35 (d, $^3J=8.34$ Hz, 2H; H_{ar}), 7.23 (d, $^3J=8.34$ Hz, 2H; H_{ar}), 4.47 (q, $^3J=7.07$ Hz, 4H; OCH_2CH_3), 4.35 (m, 10H; NCH_3 and H^1), 4.25 (s, 2H; CH_2), 3.90 (t, $^3J=4.55$ Hz, 4H; H^2), 3.73 (d, $^3J=6.1$ Hz and d, $^3J=4.8$ Hz, 4H; $H^{3,4}$), 3.68–3.64 (m, 8H; H^2, $H^{3,4}$ and $H^{5,6}$), 3.52 (t, $^3J=5.05$ Hz, 4H; $H^{5,6}$), 3.35 (s, OCH_3; 6H), 1.44 ppm (t, $^3J=7.07$ Hz, 6H; OCH_2CH_3). ^{13}C NMR (600 MHz, $CDCl_3$): $\delta=166.37$ (C_{ar}-O), 164.75 (C=O), 152.05 (C_{ar}), 149.14 (C_{ar}), 148.52 (C_{ar}), 142.35 (C_{ar}), 136.46, (C_{ar}) 135.90 (C_{ar}), 125.05 (CH_{ar}), 119.68 (CH_{ar}), 113.23 (CH_{ar}), 111.75 (CH_{ar}), 109.89 (CH_{ar}), 70.82 (OCH_2), 70.50 (OCH_2), 70.45 (OCH_2), 69.09 (OCH_2), 69.02 (OCH_2), 68.10 (OCH_2), 61.79 (OCH_2CH_3), 58.99 (OCH_3), 42.10 (CH_2), 32.83 (NCH_3), 14.14 ppm (OCH_2CH_3). ESI-MS m/z calcd for $[M+H^+]$: 899.41; found (899.81). calcd for $[M+2H^+]/2$: 450.21; found 450.32.

Synthesis of H_2L^{C2}: Compound **7** (220 mg, 0.24 mmol, 30 equiv) was dissolved in EtOH (0.2 mL), then NaOH (50 mL, 0.02 M) was added and the solution was heated to 60°C for 2 h. The evolution of the reaction was followed by TLC (silica plate; CH_2Cl_2/MeOH 97/3 v/v). After completion of the reaction, the basic aqueous solution was washed three times with 50 mL of CH_2Cl_2, acidified to pH 2.0 with 0.02 M HCl and extracted with four 50-mL portions of CH_2Cl_2. The organic phase was dried with Na_2SO_4 and evaporated. The ligand was further purified by column chromatography (silica gel; MeCN/NH_4OH, 100/0→88/12 v/v) to give a pale-yellow solid (164 mg, 80%). ^{1}H NMR (600 MHz, MeOD): $\delta=7.84$ (d, $^3J=2.18$ Hz, 2H; H_{ar}), 7.72 (d, $^3J=2.18$ Hz, 2H; H_{ar}), 7.61 (d, $^3J=8.55$ Hz, 2H; H_{ar}), 7.55 (d, $^3J=8.55$ Hz, 2H; H_{ar}), 7.33 (d, $^3J=8.55$ Hz, 1H; H_{ar}), 4.39 (d, $^3J=4.37$ Hz, 4H; H^1), 4.30 (s, 2H; CH_2), 4.29 (s, 6H; NCH_3), 3.95 (t, $^3J=4.37$ Hz, 4H; H^2), 3.74 (d, $^3J=6.4$ Hz and d, $^3J=5.0$ Hz, 4H; $H^{3,4}$), 3.68 (d, $^3J=6.4$ Hz and d, $^3J=5.0$ Hz, 4H; $H^{3,4}$), 3.64 (d, $^3J=6.4$ Hz and d, $^3J=5.0$ Hz, 4H; $H^{5,6}$), 3.52 (d, $^3J=6.4$ Hz and d, $^3J=5.0$ Hz, 4H; $H^{5,6}$), 3.35 ppm (s, OCH_3; 6H). ^{13}C NMR (600 MHz, MeOD): $\delta=171.78$ (C=O), 168.52 (C_{ar}-O), 156.75 (C_{ar}), 152.25 (C_{ar}), 143.55 (C_{ar}), 138.99 (C_{ar}), 137.33 (C_{ar}), 126.92 (CH_{ar}), 120.21 (CH_{ar}), 113.56 (CH_{ar}), 112.94 (CH_{ar}), 112.09 (CH_{ar}), 73.43 (OCH_2), 72.33 (OCH_2), 72.06 (OCH_2), 71.89 (OCH_2), 70.90 (OCH_2), 69.78 (OCH_2), 59.55 (OCH_3), 43.49 (CH_2), 33.73 ppm (NCH_3). ESI-MS m/z calcd for $[M+H^+]$: 843.35; found 843.37. calcd for $[M+2H^+]/2$: 422.17; found 422.37. Elemental analysis (%) calcd for $C_{43}H_{50}N_6O_{12}\cdot NH_4OH\cdot 0.5H_2O$: C 58.21, H 6.37, N 11.06; found: C 58.23, H 6.23, N 10.83.

Cell lines: The human cervical adenocarcinoma cell line HeLa (ATCC CCL-2), the mouse hybridoma cell line 5D10 (a gift from Prof. Dr. J. Raus of the Biomedical Research Institute "Dr. L. Willems-Instituut", University of Hasselt, Belgium), the human T leukaemia cell line Jurkat (ATCC TIB152) and the human breast adenocarcinoma cell line MCF-7 (ATCC HTB-22) were used in this study. Cells were cultivated in 75-cm^2 culture flasks using RPMI 1640 supplemented with 5% foetal calf serum (FCS), 2 mM L-glutamine, 1 mM sodium pyruvate, 1% non-essential amino acids, 1% 4-(2-hydroxyethyl)-1-piperazineethanesulfonic acid monosodium salt (HEPES) (all from Gibco® Cell Culture, Invitrogen, Basel, Switzerland). Cultures were maintained at 37°C under 5% CO_2 and 95% air atmosphere. The growth medium was changed every other day until the time of use of the cells. The cell density and viability, defined as the ratio of the number of viable cells over the total number of cells, of the cultures were determined by trypan blue staining and with a Neubauer improved hemacytometer (Blau Brand, Wertheim, Germany).

WST-1 cell-proliferation assay:[80,81] Cells were seeded in a 96-well tissue culture microplate at a concentration of between 1 and 5×10^5 cells per well in 100 μL of culture medium and incubated overnight at 37°C and 5% CO_2. The complex was dissolved in fresh RPMI medium at 37°C, at a concentration of 500 μM. The medium was removed from the cell cultures and 100 μL per well of the complex was added (final concentrations: 500, 250, 125 and 50 μM). WST-1 reagent (10 μL, Cell Proliferation Reagent, Roche, Germany) was added to each well and the plate was shaken for 1 min on a microtiter plate shaker (450 rpm). The plate was further incubated at 37°C and 5% CO_2 and the absorbance of the formazan product was measured at 450 nm with an ELISA reader (Spectra MAX 340, Molecular Devices, Sunnyvale, CA, USA). The cell viability [Eq. (9)] was calculated as the average of three nominally identical measurements from the absorbance difference ($A_{450}-A_{650}$) between 450 and 650 nm for the cells that were in contact with the complex (exp) and the medium:

$$\text{viability } [\%] = \frac{(A_{450}-A_{650})_{exp}}{(A_{450}-A_{650})_{medium}} \times 100 \qquad (9)$$

Live-cell imaging: For luminescence microscopy, cells were seeded on glass-bottomed cell culture dishes and loaded with the complex dissolved in freshly prepared cell culture medium. The incubation time varied from 15 min to 24 h, and the concentration of the added complex was in the range 10–500 μM. Cells were incubated at 37 or 4°C for the indicated time and washed at least six times with PBS before examination under a luminescence microscope. The cells were examined with a Zeiss luminescence microscope Axiovert S 100 (lens: Plan-Neofluar 20x/0.4 Korr Ph2 or 40x/0.60 Korr Ph2). Excitation was at 330 or 365 nm (BP 80 nm) for the Ln^{III} helicates, 470 nm (BP 40 nm) for acridine orange (AO), BODIPY FL labeled LDL or Transferrin, and the emission filters used were LP 585 nm for Eu^{III} and Sm^{III}, BP 545 (35 nm) for Tb^{III}, and BP 515–565 nm for the organic dyes; exposure times varied from 30 ms (AO) to 60 s. Confocal images were recorded with a Zeiss LSM 500 Meta microscope fitted with a Plan-Apochromat 63/1.30 oil objective; Eu luminescence was excited at 405 nm and measured through a LP 505 filter.

Concentration of intracellular $[Eu_2(L^{C2})_3]$: All incubations for the DELFIA® assay were carried out at room temperature with stirring and a final volume of 200 μL. HeLa cells were cultivated in six-well cell-culture plates and loaded overnight with $[Eu_2(L^{C2})_3]$ (25 μM) dissolved in fresh cell culture medium at 37°C. The cells were washed with PBS at least 10 times and harvested by trypsin treatment. The number of labeled cells suspended in a known volume of PBS was counted by trypan blue staining and with a Neubauer improved hemacytometer (Blau Brand, Wertheim, Germany). Cells were seeded at 50, 500 and 1000 cells per 100 μL in a 96-well Delfia® plate and 100 μL of Delfia® Inducer was added to induce complete cell lysis. The plate was shaken vigorously for 5 min and was read with a 1234 Delfia® fluorometer plate reader (Perkin–Elmer) using a europium protocol ($\lambda_{ex}=320$ nm, $\lambda_{em}=615$ nm, 400-μs delay, 1 ms integration time per cycle). To generate a calibration curve, a known number of cells in 100 μL were spiked with 100 μL of 1 μM to 1 pM $[Eu_2(L^{C2})_3]$ in Delfia® Inducer and the Eu luminescence was measured as above. Each point is the average of three or four nominally equivalent experiments.

Acknowledgments

This research was supported by a grant from the Swiss National Science Foundation (200020-107449/1). We also acknowledge selected funding by the ESF-COST D-38 Action. We thank Frédéric Thomas and Loïc Wagnières for their help in the synthesis of the ligand, as well as Frédéric Gumy for contributing to the gathering of photophysical data.

[1] N. Johnsson, K. Johnsson, *ACS Chem. Biol.* **2007**, *2*, 31–38.
[2] D. Parker, *Coord. Chem. Rev.* **2000**, *205*, 109–130.
[3] B. Song, G. Wang, M. Tan, J. Yuan, *J. Am. Chem. Soc.* **2006**, *128*, 13442–13450.
[4] J. Inglese, P. Samama, S. Patel, J. Burbaum, I. L. Stroke, K. C. Appell, *Biochemistry* **1998**, *37*, 2372–2377.
[5] R. Weissleder, *Nat. Biotech.* **2001**, *19*, 316–317.
[6] R. Weissleder, V. Ntziachristos, *Nat. Med.* **2003**, *9*, 123–128.
[7] J.-C. G. Bünzli, *Acc. Chem. Res.* **2006**, *39*, 53–61.
[8] T. Lövgren, I. Hemmilä, K. Pettersson and P. Halonen in *Alternative immunoassays* (Ed.: W. P. Collins), John Wiley & Sons, New York, **1985**, chap. 12.
[9] I. Hemmilä, T. Ståhlberg and P. Mottram, *Bioanalytical Applications of Labelling Technologies*, Wallac Oy, Turku, **1995**.
[10] I. Hemmilä, V. M. Mukkala, *Crit. Rev. Clin. Lab. Sci.* **2001**, *38*, 441–519.
[11] V. W. W. Yam, K. K. W. Lo, *Coord. Chem. Rev.* **1999**, *184*, 157–240.
[12] S. Comby, and J.-C. G. Bünzli, *Lanthanide Near-Infrared Luminescence in Molecular Probes and Devices*, Handbook on the Physics and Chemistry of Rare Earths, Elsevier Science B. V., Amsterdam, **2007**, Vol. 37, chap. 235,
[13] S. Faulkner, S. J. A. Pope, B. P. Burton-Pye, *Appl. Spectrosc. Rev.* **2005**, *40*, 1–31.
[14] G. Piszczek, I. Gryczynski, B. P. Maliwal, J. R. Lakowicz, *J. Fluoresc.* **2002**, *12*, 15–17.
[15] R. A. Poole, C. P. Montgomery, E. J. New, A. Congreve, D. Parker, M. Botta, *Org. Biomol. Chem.* **2007**, *5*, 2055–2062.
[16] H. Bazin, E. Trinquet, G. Mathis, *Rev. Mol. Biotechnol.* **2002**, *82*, 233–250.
[17] S. Pandya, J. H. Yu, D. Parker, *Dalton Trans.* **2006**, 2757–2766.
[18] D. J. Bornhop, D. S. Hubbard, M. P. Houlne, C. Adair, G. E. Kiefer, B. C. Pence, D. L. Morgan, *Anal. Chem.* **1999**, *71*, 2607–2615.
[19] I. Nasso, C. Galaup, F. Havas, P. Tisnes, C. Picard, S. Laurent, L. V. Elst, R. N. Muller, *Inorg. Chem.* **2005**, *44*, 8293–8305.
[20] K. Matsumoto and J. G. Yuan, *Lanthanide Chelates as Fluorescent Labels for Diagnostics and Biotechnology*, Metal Ions in Biological Systems (Eds.: A. Sigel and H. Sigel), Marcel Dekker Inc., New York, **2003**, Vol. 40, chap. 6,
[21] W. L. Scaff, D. L. Dyer, K. Mori, *J. Bacteriol.* **1969**, *98*, 246–248.
[22] S. Phimphivong, S. S. Saavedra, *Bioconjug. Chem.* **1998**, *9*, 350–357.
[23] M. I. Gaiduck, V. V. Grigor′yants, A. F. Mironov, V. D. Rumyantseva, V. I. Chissov, G. M. Sukhin, *J. Photochem. Photobiol. B* **1990**, *7*, 15–20.
[24] H. Y. D. Ke, E. R. Birnbaum, D. W. Darnall, P. J. Jackson, G. D. Rayson, *Appl. Spectrosc.* **1992**, *46*, 479–488.
[25] O. Zohar, M. Ikeda, H. Shinagawa, H. Inoue, H. Nakamura, D. Elbaum, D. L. Alkon, T. Yoshioka, *Biophys. J.* **1998**, *74*, 82–89.
[26] D. J. Bornhop, J. M. M. Griffin, T. S. Goebel, M. R. Sudduth, B. Bell, M. Motamedi, *Appl. Spectrosc.* **2003**, *57*, 1216–1222.
[27] M. P. Houlne, T. S. Agent, G. E. Kiefer, K. McMilian, D. J. Bornhop, *Appl. Spectrosc.* **1996**, *50*, 1221–1228.
[28] J. H. Yu, D. Parker, R. Pal, R. A. Poole, M. J. Cann, *J. Am. Chem. Soc.* **2006**, *128*, 2294–2299.
[29] R. A. Poole, G. Bobba, M. J. Cann, J. C. Frias, D. Parker, R. D. Peacock, *Org. Biomol. Chem.* **2005**, *3*, 1013–1024.
[30] Y. Bretonniere, M. J. Cann, D. Parker, R. Slater, *Org. Biomol. Chem.* **2004**, *2*, 1624–1632.
[31] C. Piguet and C. F. G. C. Geraldes, *Paramagnetic NMR lanthanide Induced Shifts for Extracting Solution Structures*, Handbook on the Physics and Chemistry and Rare Earths, Elsevier Science, Amsterdam, **2003**, Vol. 33, chap. 215.
[32] G. Pintacuda, M. John, X. C. Su, G. Otting, *Acc. Chem. Res.* **2007**, *40*, 206–212.
[33] M. Bottrill, L. K. Nicholas, N. J. Long, *Chem. Soc. Rev.* **2006**, *35*, 557–571.
[34] M. Woods, E. W. C. Donald, A. D. Sherry, *Chem. Soc. Rev.* **2006**, *35*, 500–511.
[35] M. M. Huber, A. B. Staubli, K. Kustedjo, M. H. B. Grey, J. Shih, S. E. Fraser, R. E. Jacobs, T. J. Meade, *Bioconjug. Chem.* **1998**, *9*, 242–249.
[36] H. C. Manning, T. Goebel, R. C. Thompson, R. R. Price, H. Lee, D. J. Bornhop, *Bioconjug. Chem.* **2004**, *15*, 1488–1495.
[37] Q. Zheng, H. Dai, M. E. Merritt, C. Malloy, C. Y. Pan, W. H. Li, *J. Am. Chem. Soc.* **2005**, *127*, 16178–16188.
[38] C. Picard, N. Geum, I. Nasso, B. Mestre, P. Tisnes, S. Laurent, R. N. Muller, L. Vander Elst, *Bioorg. Med. Chem. Lett.* **2006**, *16*, 5309–5312.
[39] R. J. Aarons, J. K. Notta, M. M. Meloni, J. Feng, R. Vidyasagar, J. Narvainen, S. Allan, N. Spencer, R. A. Kauppinen, J. S. Snaith, S. Faulkner, *Chem. Commun.* **2006**, 909–911.
[40] L. J. Martin, M. J. Hahnke, M. Nitz, J. Wohnert, N. R. Silvaggi, K. N. Allen, H. Schwalbe, B. Imperiali, *J. Am. Chem. Soc.* **2007**, *129*, 7106–7113.
[41] N. R. Silvaggi, L. J. Martin, H. Schwalbe, B. Imperiali, K. N. Allen, *J. Am. Chem. Soc.* **2007**, *129*, 7114–7120.
[42] J.-C. G. Bünzli, C. Piguet, *Chem. Rev.* **2002**, *102*, 1897–1928.
[43] C. Piguet, G. Bernardinelli, G. Hopfgartner, *Chem. Rev.* **1997**, *97*, 2005–2062.
[44] N. André, T. B. Jensen, R. Scopelliti, D. Imbert, M. Elhabiri, G. Hopfgartner, C. Piguet, J.-C. G. Bünzli, *Inorg. Chem.* **2004**, *43*, 515–529.
[45] T. B. Jensen, R. Scopelliti, J.-C. G. Bünzli, *Inorg. Chem.* **2006**, *45*, 7806–7814.
[46] T. B. Jensen, R. Scopelliti, J.-C. G. Bünzli, *Chem. Eur. J.* **2007**, *13*, 8404–8410.
[47] M. Elhabiri, R. Scopelliti, J.-C. G. Bünzli, C. Piguet, *J. Am. Chem. Soc.* **1999**, *121*, 10747–10762.
[48] A.-S. Chauvin, S. Comby, B. Song, C. D. B. Vandevyver, J.-C. G. Bünzli, *Chem. Eur. J.* **2007**, *13*, 9515–9526.
[49] C. D. B. Vandevyver, A.-S. Chauvin, S. Comby, J.-C. G. Bünzli, *Chem. Commun.* **2007**, 1716–1718.
[50] M. A. Phillips, *J. Chem. Soc.* **1928**, 172–177.
[51] M. Elhabiri, J. Hamacek, J.-C. G. Bünzli, A.-M. Albrecht-Gary, *Eur. J. Inorg. Chem.* **2004**, 51–62.
[52] S. T. Frey, W. de W. Horrocks, *Inorg. Chim. Acta* **1995**, *229*, 383–390.
[53] C. Piguet, J.-C. G. Bünzli, G. Bernardinelli, G. Hopfgartner, S. Petoud, O. Schaad, *J. Am. Chem. Soc.* **1996**, *118*, 6681–6697.
[54] C. Görller-Walrand and K. Binnemans, *Rationalisation of crystal field parameterisation*, Handbook on the Physics and Chemistry of Rare Earths, (Eds.: K. A. Gschneidner, Jr. and L. Eyring), Elsevier Science, Amsterdam, **1996**, Vol. 23, chap. 155,
[55] A. Beeby, I. M. Clarkson, R. S. Dickins, S. Faulkner, D. Parker, L. Royle, A. S. de Sousa, J. A. G. Williams, M. Woods, *J. Chem. Soc. Perkin Trans. 2* **1999**, 493–503.
[56] R. M. Supkowski, W. d. W. Horrocks, *Inorg. Chim. Acta* **2002**, *340*, 44–48.
[57] S. Faulkner, A. Beeby, M.-C. Carrié, A. Dadabhoy, A. M. Kenwright, P. G. Sammes, *Inorg. Chem. Commun.* **2001**, *4*, 187–190.
[58] A. E. Martell and R. M. Smith, *Critical Stability Constants*, Plenum Press, New York, **1974**.
[59] J. Idkowiak-Baldys, K. P. Becker, K. Kitatani, Y. A. Hannun, *FASEB J.* **2006**, *20*, A483–A484.
[60] I. Chiu, D. M. Davis, J. L. Strominger, *Proc. Natl. Acad. Sci. USA* **1999**, *96*, 13944–13949.
[61] J.-C. G. Bünzli, in *Lanthanide Probes in Life, Chemical and Earth Sciences. Theory and Practice* (Eds.: J.-C. G. Bünzli and G. R. Choppin), Elsevier Science, Amsterdam, **1989**, chap. 7, pp. 219–293.

[62] S. K. Jonas, P. A. Riley, *Cell Biochem. Funct.* **1991**, *9*, 245–253.
[63] P. Atkinson, B. S. Murray, D. Parker, *Org. Biomol. Chem.* **2006**, *4*, 3166–3171.
[64] R. Pal, D. Parker, *Chem. Commun.* **2007**, 474–476.
[65] J. C. Frias, G. Bobba, M. J. Cann, C. J. Hutchison, D. Parker, *Org. Biomol. Chem.* **2003**, *1*, 905–907.
[66] K. Melikov, L. Chernomordik, *Cell. Mol. Life Sci.* **2005**, *62*, 2739–2749.
[67] M. H. V. Werts, R. T. F. Jukes, J. W. Verhoeven, *Phys. Chem. Chem. Phys.* **2002**, *4*, 1542–1548.
[68] C. Yang, L. M. Fu, Y. Wang, J. P. Zhang, W. T. Wong, X. C. Ai, Y. F. Qiao, B. S. Zou, L. L. Gui, *Angew. Chem.* **2004**, *116*, 5120–5123; *Angew. Chem. Int. Ed.* **2004**, *43*, 5010–5013.
[69] P. Atkinson, K. S. Findlay, F. Kielar, R. Pal, D. Parker, R. A. Poole, H. Puschmann, S. L. Richardson, P. A. Stenson, A. L. Thompson, J. H. Yu, *Org. Biomol. Chem.* **2006**, *4*, 1707–1722.
[70] A. B. Pangborn, M. A. Giardello, R. H. Grubbs, R. K. Rosen, F. J. Timmers, *Organometallics* **1996**, *15*, 1518–1520.
[71] J.-C. G. Bünzli, C. Mabillard, *Inorg. Chem.* **1986**, *25*, 2750–2754.
[72] G. Schwarzenbach, *Complexometric Titrations*, Chapman & Hall, London, **1957**.
[73] E. R. Malinowski and D. G. Howery, *Factor Analysis in Chemistry*, John Wiley, New York, Chichester, Brisbane, Toronto, **1991**.
[74] H. Gampp, M. Maeder, C. J. Meyer, A. D. Zuberbühler, *Talanta* **1985**, *32*, 257–264.
[75] H. Gampp, M. Maeder, C. J. Meyer, A. D. Zuberbühler, *Talanta* **1986**, *33*, 943–951.
[76] R. Rodriguez-Cortinas, F. Avecilla, C. Platas-Iglesias, D. Imbert, J.-C. G. Bünzli, A. de Blas, T. Rodriguez-Blas, *Inorg. Chem.* **2002**, *41*, 5336–5349.
[77] A.-S. Chauvin, F. Gumy, D. Imbert, J.-C. G. Bünzli, *Spectrosc. Lett.* **2004**, *37*, 517–532; erratum: *Spectrosc. Lett.* **2006**, *40*, 193.
[78] J. B. Lamture, Z. H. Zhou, A. S. Kumar, T. G. Wensel, *Inorg. Chem.* **1995**, *34*, 864–869.
[79] C. Piguet, G. Bernardinelli, B. Bocquet, A. Quattropani, A. F. Williams, *J. Am. Chem. Soc.* **1992**, *114*, 7440–7451.
[80] M. Ishiyama, K. Sasamoto, M. Shiga, Y. Ohkura, K. Ueno, K. Nishiyama, I. Taniguchi, *Analyst* **1995**, *120*, 113–116.
[81] M. Ishiyama, M. Shiga, K. Sasamoto, M. Mizoguchi, P. G. He, *Chem. Pharm. Bull.* **1993**, *41*, 1118–1122.

Received: August 29, 2007
Published online: December 20, 2007

